RSC Advances

This article can be cited before page numbers have been issued, to do this please use: J. Hargreaves, H. Gu, A. McFarlane and G. MacKinnon , *RSC Adv.*, 2016, DOI: 10.1039/C6RA06204K.

ROYAL SOCIETY OF CHEMISTRY

www.rsc.org/advances

View Article Online
DOI: 10.1039/C6RA06204K

The carbon deposits formed by reaction of a series of red mud samples with methanol

Hannian Gu [a], Justin S. J. Hargreaves [b*], Andrew R. McFarlane [b], Gillian MacKinnon [c]

[a] Key Laboratory of High-temperature and High-pressure Study of the Earth's Interior, Institute of Geochemistry, Chinese Academy of Sciences, Guiyang 550081, China

[b] West CHEM, School of Chemistry, University of Glasgow, Joseph Black Building, Glasgow G12 8QQ, UK

E-mail: Justin.Hargreaves@glasgow.ac.uk

[c] Scottish Universities Environmental Research Centre, Rankine Avenue, East Kilbride G75 0QF, UK

Abstract: New magnetic carbon materials were prepared by the catalytic growth of graphitic carbon and carbon nanofibers using methanol as carbon source with a series of red mud wastes from different sources. Both the raw red mud samples and products of the graphitic carbon and carbon nanofibers were characterized using powder X-ray diffraction, scanning electron microscopy, Raman spectroscopy, Brunaeur Emmett and Teller surface area analysis, thermogravimetric analysis and carbon content analysis. Hematite and goethite in high iron content red muds were reduced into magnetite in 10 minutes at 500 ^{o}C, and graphitic carbon reflections were evident in the resultant powder X-ray diffraction pattern. Thus, the samples become magnetic and change color from red to black. After six hours reaction at 500 ^{o}C, the carbon content of the composite based on a high iron content Bayer Process derived red mud reached as high as ca. 72% and its surface area increased from 17 to 312 m^2/g.

Key words: red mud; methanol; carbon deposit; iron

Introduction

Red mud is the main waste discharged during alumina extraction by means of the Bayer Process or the Sintering Alumina Process.[1-2] About 90% of the alumina produced in the world is obtained by the Bayer Process which is an effective procedure for processing high grade bauxite ores. However most local bauxite ores in China are low grade, diaspore type bauxite, for which the alternative sintering

View Article Online
DOI: 10.1039/C6RA06204K

alumina process is applied.[2-4] Historically, the treatment and disposal of red mud has posed a huge challenge for the alumina plants and the alumina industry, and have caused a significant problem leading to environmental pollution, as exemplified by the failure of the dam of the red mud reservoir in Ajka (Hungary), which collapsed in October, 2010, causing rivers and lands to be contaminated with red mud and causing ten fatalities.[5] Thus, the development of new technologies for utilization of red mud is an aspiration of great interest for the alumina industry as well as for society as a whole. Red mud has been investigated for various applications, such as construction materials,[6-7] production of ceramics,[8] gas and water purification,[4,9-10] and catalysis.[11-13]

Recent studies have demonstrated that red mud is catalytically active to produce carbon from different sources, such as methane,[14-15] ethylene,[16] ethanol,[17-18] associated petroleum gas,[19] and a crude untreated waste stream from bio-diesel production.[20] The resultant carbon materials can be used as functional materials, such as for treatment of metal-contaminated water,[21] whilst the co-product of hydrogen formed in the cracking of hydrocarbons can be used as fuel.[22]

In this study we demonstrate that using methanol as carbon resource can be used to obtain graphitic carbon and carbon nanofibers in presence of a series of red mud wastes, including high iron content red mud and low iron content red muds, and red muds from both the Bayer Process and from the Sintering Alumina Processes. Methanol has been chosen as a reactant due to its reactivity and also widespread availability given that it is mass produced on an industrial scale.

Experimental

Red mud samples from 5 different sources (1 from India, 4 from China) were used in this study, including Bayer Process derived red mud (BRM), red mud from the Sintering Process (RMS), high iron Bayer Process derived red mud and low iron content Bayer Process derived red mud. The chemical compositions were determined using an Oxford Instruments Energy 250 energy dispersive spectrometer system

View Article Online
DOI: 10.1039/C6RA06204K

(EDS). Samples for scanning electron microscopy (SEM) were sprinkled on carbon coated stubs and were coated with Pd/Au. Each sample analysis was replicated in the whole screen area, and then the average composition was obtained (Table 1). The composition of a number of the materials applied in this study have been determined by bulk analytical techniques such as inductively coupled plasma based analyses and X-ray fluorescence have been reported previously and have been found to be similar to those reported here. These samples are RM7, [14] GZ1 (referred to as PBAP), and GZ3 (referred to as GZHE) [23].

Table 1 Elemental content (wt%) of original red mud samples.

Labels	Na	Al	Si	K	Ca	Ti	Fe	Types and location
RM7	8.59	12.02	6.78	-	0.61	0.52	23.85	BRM, India
GZ1	5.45	9.50	7.10	1.40	10.74	3.30	9.23	BRM, Guizhou, China
GZ3	2.72	4.03	7.47	1.23	21.41	1.68	5.41	RMS, Guizhou, China
SD	9.43	12.28	8.69	-	-	2.61	21.15	BRM, Shandong, China
GX	5.84	7.98	6.06	-	9.45	4.21	19.86	BRM, Guangxi, China

BRM, Bayer Process derived red mud; RMS, Red mud from Sintering Process

The reactor employed for methanol cracking to deposit carbon was comprised of temperature and flow controllers, and a quartz microreactor tube inside which red mud samples (250 mg) were loaded and sat on a frit. Trace heating was applied to all reactor lines. Methanol was delivered at a rate of 0.03 ml min^{-1} and was vaporised in a flow of 25 ml min^{-1} of Ar (BOC gas) carrier. A high performance liquid chromatography pump (Knauer, K-501) was used to deliver the methanol feed.

Samples and the composite products were characterized by powder X-ray diffraction (XRD), Raman spectroscopy (λ = 532.09 nm), Brunaeur Emmett and Teller (BET) surface area analysis, CHN elemental analysis, thermogravimetric analysis TGA and SEM.

Powder X-ray diffraction measurements were performed using a Siemens D5000

View Article Online
DOI: 10.1039/C6RA06204K

diffractometer with Cu Kα radiation. A 2θ range between 5° and 85° was scanned using a counting rate of 1 s per step with a step size of 0.02°. Samples were prepared by compaction into a silicon sample holder.

The Raman Spectrometer was a LabRAM HR system, manufactured by Horiba Jobin Yvon with Ventus 532 laser system, 100 mW, 532 nm.

BET surface areas were determined where appropriate from N_2 physisorption isotherms measured at 77 K following out-gassing, using a Micromeritics Gemini. For the determination of carbon content, CHN analysis was performed by combustion using a CE 440 elemental analyzer.

TGA was performed on a TA Instruments SDT Q600 instrument. Post-reaction samples were investigated using air or N_2 (BOC gases), and a temperature ramp rate of 10 $^{o}C\ min^{-1}$ from room temperature to 1000 ^{o}C was applied.

Samples for SEM were dispersed on carbon coated stubs and were coated with Pd prior to being viewed in a Philips/FEI (XL30) scanning electron microscope with an Oxford Instruments Energy 250 energy dispersive spectrometer system (EDS).

Results and discussion

Powder X-ray diffraction was performed (Figure 1) to identify the mineral phase composition of the five original red mud samples since they are from different sources and processes and possess very different chemical compositions. As has been widely recognised,[24] red mud is always complex and multi-component in terms of composition. For the iron-containing phase, hematite can be matched in four of the five raw samples, except GZ3, the sintering process red mud. As previously reported, goethite and hematite are major crystalline components of the RM7.[15] Given the fact that the samples are complex mixtures containing a number of different components, identification of the exact composition of the red mud samples by XRD can be highly challenging and not fully reliable. Surveying the literature, major phases present in many red mud samples can be expected to be hematite, goethite and Gibbsite, along with various sodium aluminium hydrosilicates [24]. In view of the ensuing discussion,

View Article Online
DOI: 10.1039/C6RA06204K

only the predominant iron-containing phases (hematite and goethite) are marked on the patterns. A more detailed match for the RM7 sample can be found elsewhere [14]. It is apparent that the phase composition of the GZ3 sample is clearly different and in this case major reflections can be matched to the presence of calcium silicate.

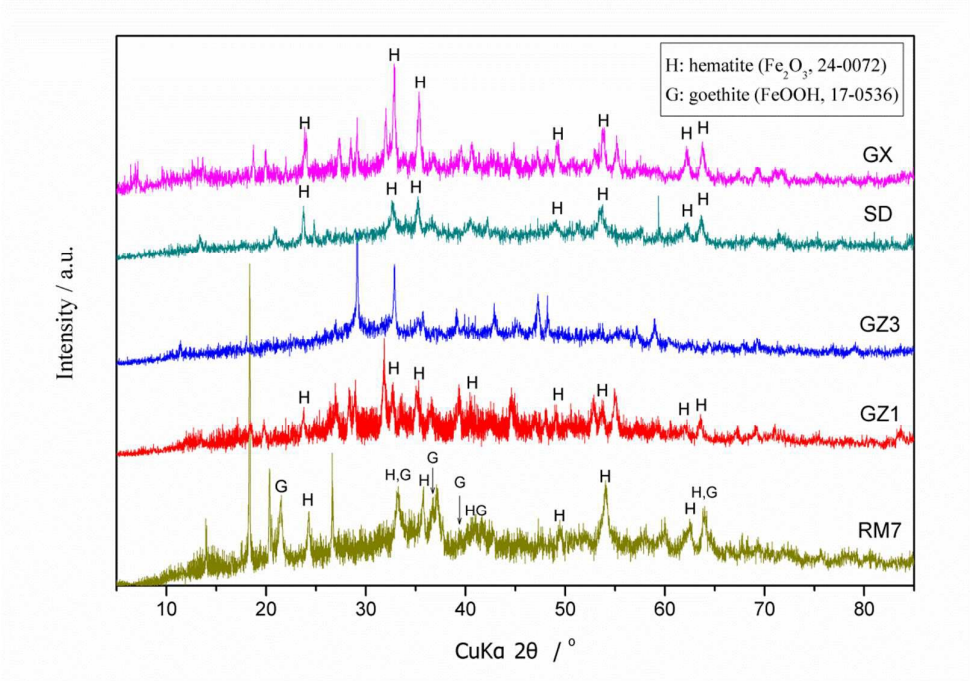

Figure 1 XRD pattern of the five raw red mud samples. H: hematite (Fe_2O_3, 24-0072); G: goethite (FeOOH, 17-0536).

Methanol cracking experiments have been performed in the presence of red mud wastes. The red mud samples were used as obtained, without any modification or pretreatment. Figure 2 shows the XRD patterns of RM7 with varying reaction time at 500 ^{o}C. After the reaction run for 10 minutes, the diffraction pattern changed significantly. Hematite and goethite were reduced into magnetite. Unlike the reaction with methane at much higher temperature,[13-14] Fe and Fe_3C were not observed as a result of the reduction of the iron oxides in red mud and methanol. Furthermore, broad carbon peaks were observed beyond 2 hours reaction, are indicative of the production

View Article Online
DOI: 10.1039/C6RA06204K

of disordered carbon. The relative intensity of magnetite peaks became weaker with the increasing reaction time because of the accumulation of carbon.

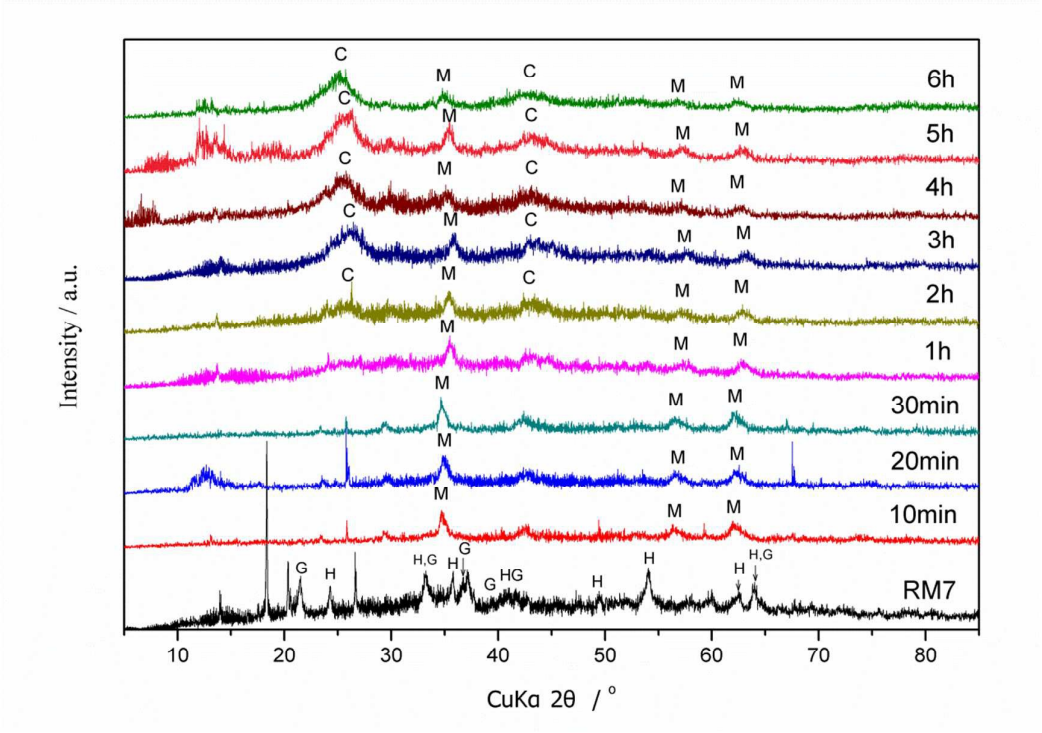

Figure 2 XRD patterns of RM7 before and after reaction with methanol the carbon deposit for different times at 500 °C. H: hematite; G: goethite; C: carbon; M magnetite

The effect of reaction time on carbon content and BET surface area for the RM7 run for different durations at 500 °C was investigated (Figure 3). Carbon deposition was apparent after the first 10 minutes of reaction. The resultant material was magnetic and with color transformation from red to black, as well as a change in BET surface area. The carbon content of the post-reaction material increased gradually from ca. 1.1% to ca. 5.8% after the first 30 minutes on stream. One hour later the carbon content increase was more marked, achieving ca. 72 wt% after six hours. In addition, the BET surface area significantly increased over the first 30 minutes of the reaction, and reached 10 times that of the original sample after 5 hours reaction, and nearly 20 times (312 m^2 g^{-1}) after 6 hours reaction compared to the original red mud. In comparison to methane, methanol is more active for the deposition of carbon when used as carbon source, as might be expected from its higher reactivity. In other studies

View Article Online
DOI: 10.1039/C6RA06204K

the carbon contents for the composites prepared up to 950 °C based on ethanol were ca. 32% (at ca. 6 vol% in N_2 with a flow of 30 ml min^{-1} using 50 mg of red mud, at 900 °C),[17] and composites formed by methane decomposition at up to 800 °C contained carbon less than 50% (at a total rate of 60 ml min^{-1} CH_4 over a ca. 0.4 g catalyst using feed gas of 80% CH_4 and 20% N_2).[14]

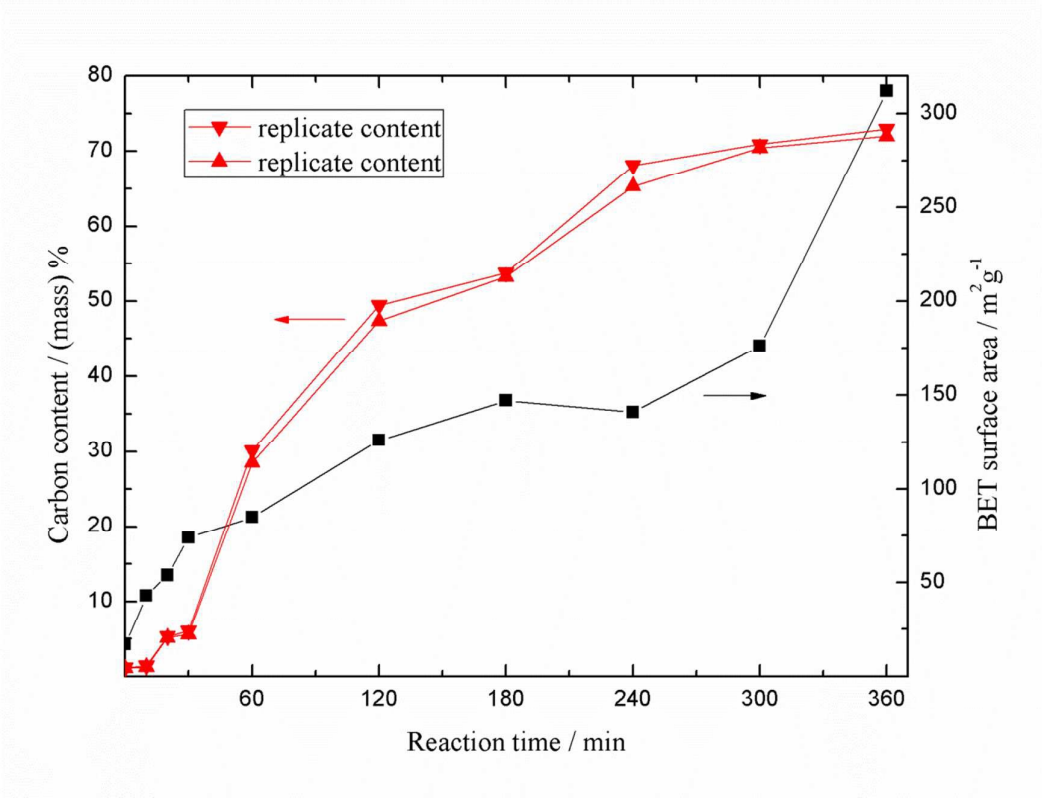

Figure 3 Effect of reaction time on carbon content and BET surface area of the products based on RM7 and methanol at 500 °C

The carbon content of different original red mud wastes and the materials reacted for 5 hours are presented in Table 2. For post-reaction samples based on RM7, which is a high iron-containing Bayer Process derived red mud, the carbon content decreased slightly after 5 hours reaction with methanol at the temperature of 400 °C. At 450 °C the content increased significantly, achieving ca. 54%, then 70% at 500 °C, and then decreased slightly to ca. 60% at 550 °C. A similar tendency was observed for the composites based on GX. Thus, the results of carbon content indicate that the higher carbonizing temperature cannot always generate a better effect than lower temperature

View Article Online
DOI: 10.1039/C6RA06204K

for the methanol cracking process since loss of carbon by gasification may be possible when using a water producing reactant. In the case of the low iron-containing samples, such as Bayer Process derived red mud, GZ1 (carbon wt% of 1.28-1.41%), and the sintering process red mud, GZ3 (carbon wt% of 1.96-2.08%), after 5 h 500 ^{o}C reaction the final products only reached 4%. The low carbon content can be accounted for by the iron contents in the original red mud samples, which suggests that the iron content dominates the amount of carbon deposited. In terms of the behavior of GZ1 and GZ3, it can be concluded that the compositional variation seems to have no effect on the amount of carbon. Thus, components other than iron in red mud are also responsible for the amount of carbon deposition.

Table 2 Replicate carbon contents of raw red mud reacted for 5 hours at different reaction temperatures

Reaction temperature (^{o}C)	Carbon content after 5h reaction with methanol (%)				
	RM7	GZ1	GZ3	SD	GX
Original RM	1.06/1.11	1.28/1.41	1.96/2.08	0.73/0.89	1.22/1.27
400	0.87/1.00	1.60/1.67	2.06/2.18	4.42/4.61	5.89/6.02
450	54.02/54.69	2.34/2.35	2.49/2.69	40.95/41.15	51.27/51.42
500	70.44/70.92	3.95/4.21	3.64/3.93	44.91/45.78	52.32/57.39
550	60.30/60.32	4.42/4.66	7.11/7.34	67.41/67.88	38.33/38.58

Figure 4 presents the Raman spectra in the carbon fingerprint region for RM7 run at 500 ^{o}C with varying reaction time. The main features in Raman spectra of carbon materials are G and D peaks. In this case the intensity of D peaks (at around 1340 cm^{-1}) is stronger than the G peaks (around 1590 cm^{-1}), whereas for GZ1 and GZ3, the opposite trend is evident (Figure 5). For the Raman pattern of resultants based on GZ1 and GZ3, the relative intensity of the G peaks (around 1595 cm^{-1}) is greater than the D peaks (at around 1325 cm^{-1}), which is indicative of a lower degree of disorder. Figure 5 also gives the characterisation of the products based on SD and GX, indicating the value of I(D)/I(G) is more than 1.0, which are quite similar to the post-reaction samples of RM7. These phenomena suggested that carbons based on RM7, SD and GX, were disordered graphitic carbon, and those from GZ1 and GZ3 may be more

View Article Online
DOI: 10.1039/C6RA06204K

ordered. As already discussed, the high iron RM7 was much more reactive for the deposition of carbon than the low iron samples of GZ1 and GZ3 under the same reaction conditions.

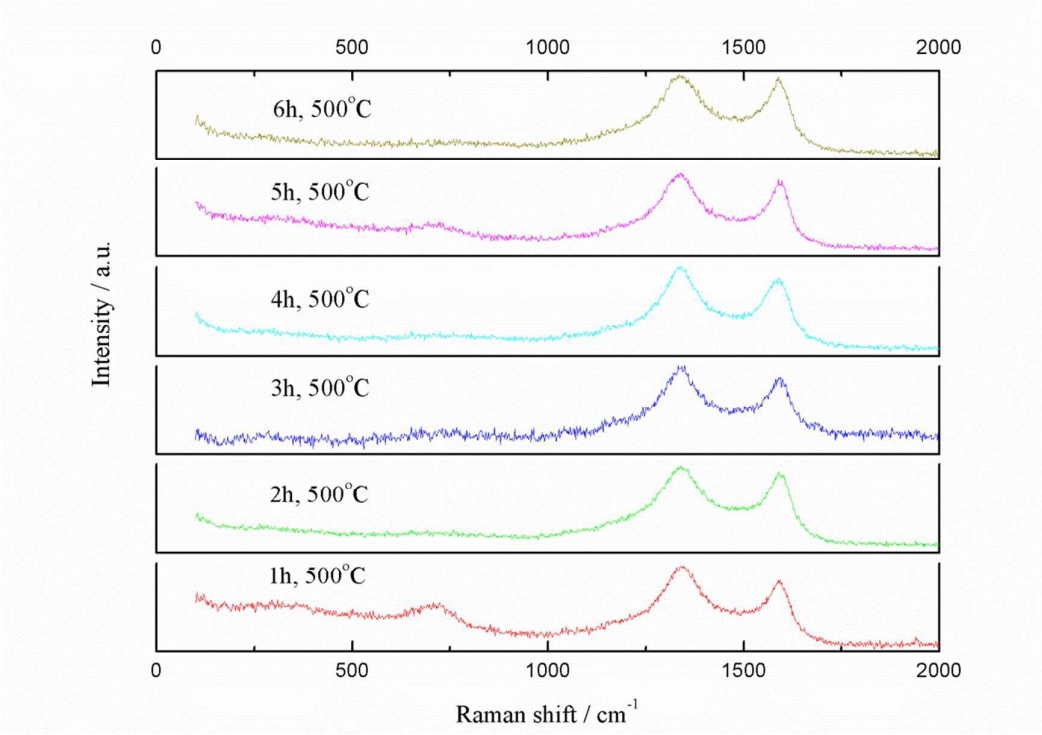

Figure 4 Raman spectra of the carbon region for different reaction times for RM7.

View Article Online
DOI: 10.1039/C6RA06204K

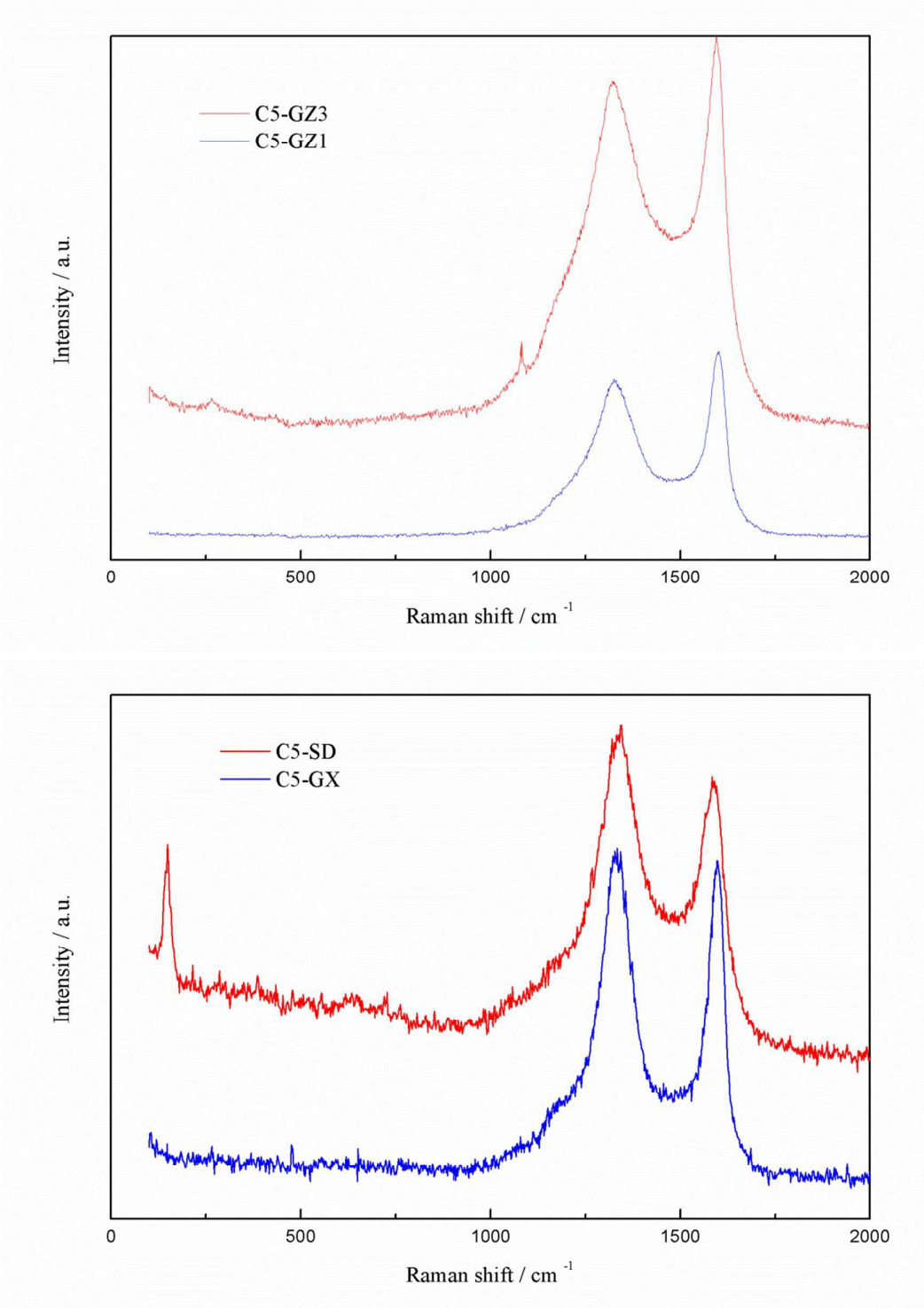

Figure 5 Raman spectra following the 5-hour reactions at 500 ^{o}C for GZ1, GZ3, SD and GX.

TGA oxidation studies were carried out to investigate the reactivity of the carbon species and to verify the carbon content. Curves from RM7 materials reacted from 1 hour to 6 hours at 500 ^{o}C are shown in Figure 6. The total mass decrease can be

View Article Online
DOI: 10.1039/C6RA06204K

attributed to oxidation of carbon and is, in reasonable agreement with the CHN analysis. All the curves show a slight mass increase up to around 400 °C followed by a sudden drop in the weight for thermal degradation of the material, and an abrupt change in the slope (except the 1h sample), leading to a slower weight loss in the temperature range 450/490 to 560/590 °C. The mass increase stage was previously explained by oxidation of the reduced phases generated by the reaction of RM7 and methane.[13] In this study, the slight increase can be attributed to oxidation of magnetite produced from precursor hematite or goethite phases. It is known that magnetite can be oxidized below 400 °C.[25] From 2 hours reaction time onwards, the carbon species were oxidized in two stages, which may mean that two different carbon species were generated during the methanol cracking process.

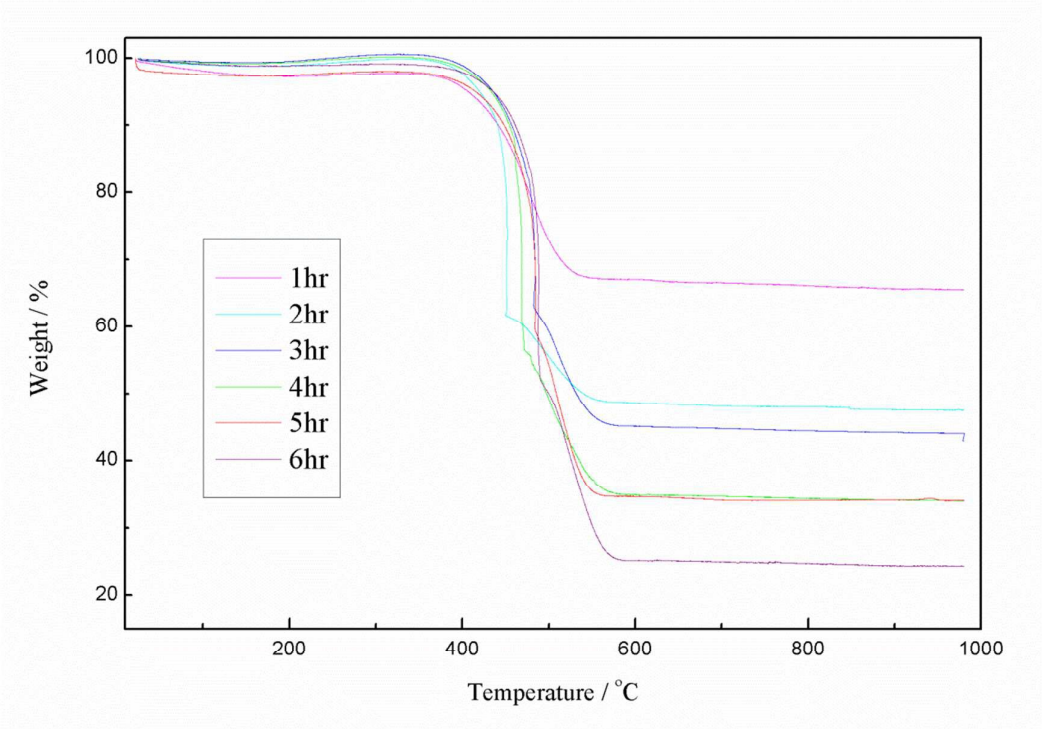

Figure 6 TGA analysis of RM7 derived products as a function of different reaction times.

TGA curves of samples based on GZ1 and GZ3 show a slight mass increase up to around 500 °C before a sudden drop in the weight due to oxidation of carbon (Figure 7). Like the Raman spectra, TGA curves based on SD and GX (Figure 7) are also similar to the samples based on RM7.

View Article Online
DOI: 10.1039/C6RA06204K

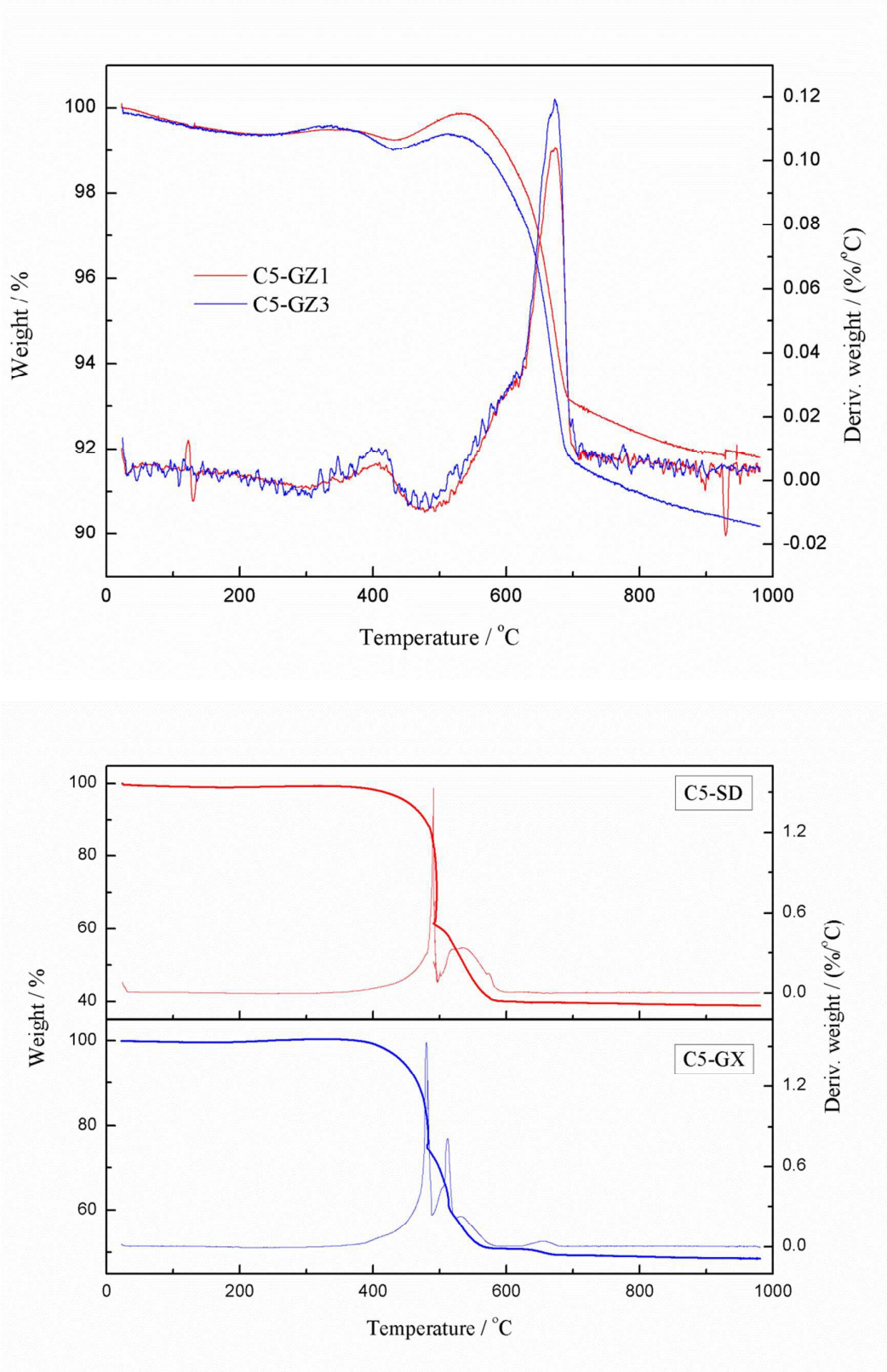

Figure 7 TGA analysis after 5 hours reaction at 500 °C based on GZ1, GZ3, SD and GX.

View Article Online
DOI: 10.1039/C6RA06204K

From SEM observation, it appears that there are two types of carbon product based on RM7. One is large sheets of graphitic carbon, and the other is a carbon fiber with a nano-scale diameter (Figure 8). From SEM observations, the first stage appearing from 2 to 6 h reaction time, is due to the formational of disordered graphitic carbons, which are lost in the TGA studies at lower temperature because of their disorder. The second stage of the TGA may be related to nano-scaled fibers, which are not present in the sample run for 1h. In general the mass normalized surface areas obtained in this study are lower than is the case for activated carbons (where areas of >1000 m^2g^{-1} may occur.) This may be due to both the fact that the composites also comprise low surface area dense components resulting from the transformation of the red muds and also that the proportion of the large graphitic sheet component is relatively high.

The results in this study demonstrate that the iron components are important for the growth of the carbon from reaction with methanol. The presence of iron components also imparts magnetic behavior to the resultant composites which can facilitate their application in, for example, water remediation for which carbonized RM7 has been shown to be of greater interest than its parent red mud counterpart [26]. In addition to acting as sorbents, the resultant carbonized composites could be used as catalyst supports or further functionalized to impart higher reactivity. The approach taken in this study has been to apply raw red mud samples directly. Given the findings of this study, this will necessarily lead to variability of product composites reflecting the variation of red mud composition. Such variability may be tolerable for high iron content red muds when account is taken of the ease of their direct application, otherwise procedures aimed at the selective extraction of iron containing components, such as the use of oxalic acid [27], may be a better strategy for the preparation of more uniform materials. Overall, given the vast amount of red mud produced annually, its use for the preparation of carbon composite materials would only have a very limited impact and would necessarily be a relatively minor part of a multi-component solution. However, red mud can be used as a cheap and readily available pre-catalyst, the utilization of which would have an impact upon

View Article Online
DOI: 10.1039/C6RA06204K

sustainability.

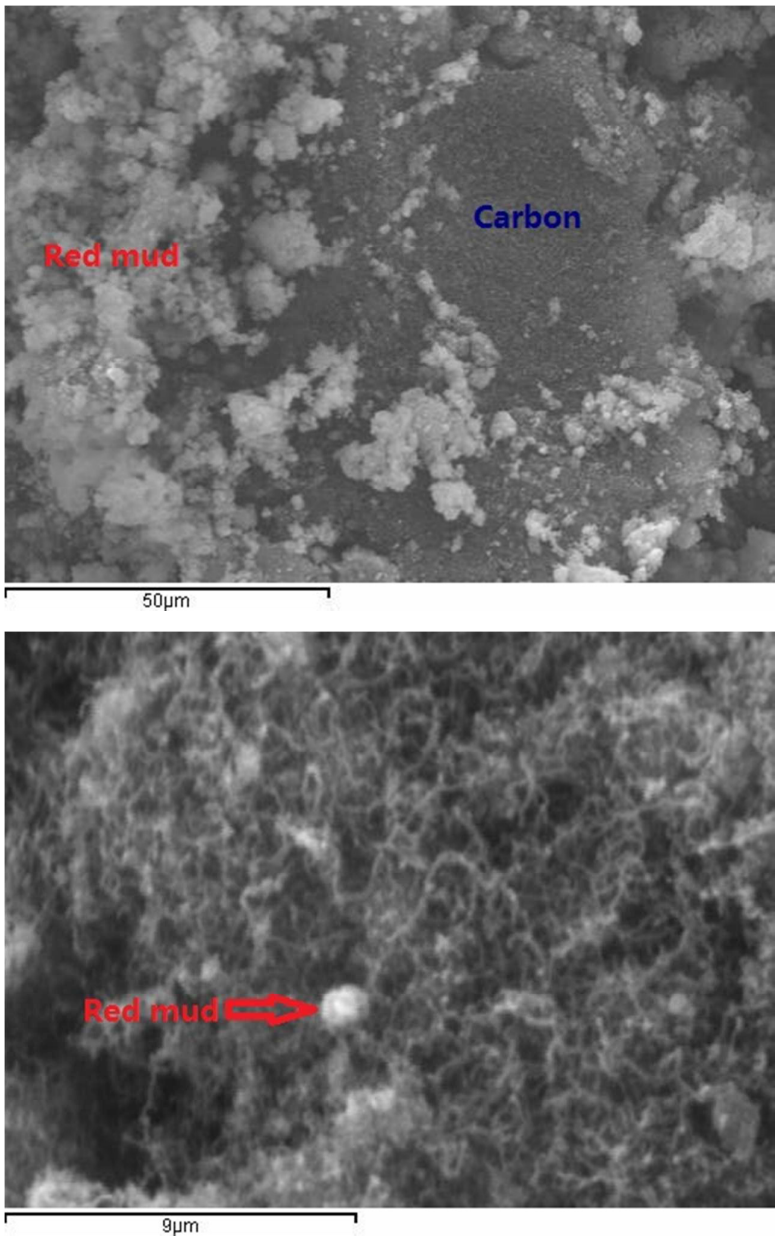

Figure 8 Morphology of magnetic carbon containing materials based on RM7.

View Article Online
DOI: 10.1039/C6RA06204K

Conclusion

It has been demonstrated that red mud waste from a variety of sources prepared using different processes are active for methanol cracking to generate composite products, comprising graphitic carbon and carbon nanofibers. The carbon content of post-reaction can be related with the iron content of the original red mud samples. However, iron is not the only factor that affects the carbon deposition. After 5 hours, 500 ^{o}C reaction with methanol, high iron-containing Bayer Process derived red muds, eg. RM7, SD and GX, can be used to generate composites with carbon content of ca. 70%, 45% and 54%, respectively, while for the low iron-containing wastes, GZ1 (Bayer Process derived red mud) and GZ3 (red mud from the sintering process), the final products only reached ca. 4.1% and ca. 3.8%, respectively.

Acknowledgements

The authors would like to acknowledge financial support from the National Natural Science Foundation of China (Grant No. 41402039) and H. Gu is thankful to the China Scholarship Council. The authors acknowledge Dr. W. Liu who provided the samples of SD and GX. We also wish to express our great appreciation to Dr. Vidya Batra from TERI University, New Dehli, for the provision of Sample RM7.

View Article Online
DOI: 10.1039/C6RA06204K

References

1. C. Klauber, M. Gräfe, G. Power. Hydrometallurgy, 2011,108, 11-32.
2. Y. Liu, C. Lin and Y. Wu, J. Hazard. Mater., 2007,146, 255-261.
3. W. Liu, J. Yang and B. Xiao, Int. J. Miner. Process, 2009, 93, 220-231.
4. L. Zhang, H. Zhang, W. Guo and Y. Tian, Appl. Clay Sci., 2014, 93-94, 85-93.
5. S. Ruyters, J. Mertens, E. Vassilieva, B. Dehandschutter, A. Poffijn and E. Smolders, Environ. Sci. Technol., 2011, 45, 1616-1622.
6. M. Singh, S.N. Upadhayay and P.M. Prasad, Waste Manage., 1996, 16, 665-670.
7. E.P. Manfroi, M. Cheriaf, J.C. and Rocha, Constr. Build. Mater., 2014, 67, 29-36.
8. Sglavo VM, Maurina S, Conci A, Salviati A, Carturan G, Cocco G, J. Eur. Ceram. Soc., 2000, 20, 245-252.
9. G. Lv, L. Wu, L. Liao, Y. Zhang and Z. Li, Appl. Clay Sci., 2013, 74, 95-101.
10. M. K. Sahu, U. K. Sahu and R. K. Patel, RSC Adv., 2015, 5, 42294-42304.
11. S. Ordóñez, H. Sastre and F. Díez, Appl. Catal. B - Environ., 2001, 29, 263-273.
12. S. Sushil, V.S. Batra, Applied Catalysis B: Environmental, 2008, 81, 64-77.
13. J.R. Kastner, R. Hilten, J. Weber, A.R. McFarlane, J.S.J. Hargreaves, V.S. Batra, RSC Adv., 2015, 5, 29375-29385.
14. M. Balakrishnan, V.S. Batra, J.S.J. Hargreaves, A. Monaghan, I.D. Pulford, J.L. Rico and S. Sushil, Green Chem., 2009, 11, 42-47.
15. S. Sushil, A.M. Alabdulrahman, M. Balakrishnan, V.S. Batra, R.A. Blackley, J. Clapp, J.S.J. Hargreaves, A. Monaghan, I.D. Pulford, J.L. Rico and W. Zhou, J. Hazard. Mater., 2010, 180, 409-18.
16. O.M. Dunens, K.J. MacKenzie and A.T. Harris, Carbon, 2010,48, 2375-7.
17. A.A.S. Oliveira, I.F. Teixeira, L.P. Ribeiro, J.C.Tristão, A. Dias and R.M. Lago, J. Brazil. Chem. Soc., 2010, 21(12), 2184-2188.
18. A.A.S. Oliveira, J.C. Tristão, J.D. Ardisson, A. Dias and R.M. Lago, Appl. Catal. B - Environ., 2011, 105, 163-170.
19. I.F. Teixeira, T.P.V. Medeiros, P.E. Freitas, M.G. Rosmaninho, J.D. Ardisson and R.M. Lago, Fuel, 2014, 124, 7-13.

View Article Online
DOI: 10.1039/C6RA06204K

20. E.C.D Resende, C. Gissane, R. Nicol, R.J. Heck, M.C. Guerreiro, J.V. Coelho, L.C.A.D. Oliveira, P. Palmisano, F. Berruti, C. Briens and M. Schlaf, Green Chem., 2013, 15, 496-510.
21. I.D. Pulford, J.S.J. Hargreaves, J. Ďurišová, B. Kramulova, C. Girard, M. Balakrishnan, V.S. Batra and J.L. Rico, J. Environ. Manage., 2012, 100, 59-64.
22. M.G. Rosmaninho, F.C.C. Moura, L.R. Souza, R.K. Nogueira, G.M. Gomes, J.S. Nascimento, M.C. Pereira, J.D. Fabris, J.D. Ardisson, M.S. Nazzarro, K. Sapag, M.H. Araújo and R.M.Lago, Catal. B - Environ., 2012, 115-116, 45-52.
23. H. Gu, N. Wang, S. Liu. Waste Manage Res, 2012, 30(9), 961-965.
24. G. Bánvölgy and T. M. Huan, Proceedings of the XVIII International Symposium of ICSOBA 25th – 27th November 2010, Zhengahoo, China, 441
25. U. Colombo, F. Gazzarrini, G. Lanzavecchia and G. Sironi, Science, 1965, 147, 1033.
26. I. D. Pulford, J. S. J. Hargreaves. J. Durisova, B. Kramulova, C. Girard, M. Balakrishnan. V. S. Batra and J. L. Rico, J. Env. Manage., 2012, 100, 59.
27. Y. yang, X. Wang, M. Wang, H. Wang and P. Xian, Hydrometall., 2015, 157, 239.